NURETH14-179

SODIUM EXPERIMENT ON FULLY NATURAL CIRCULATION SYSTEMS FOR DECAY HEAT REMOVAL IN JAPAN SODIUM-COOLED FAST REACTOR

**H. Kamide¹, J. Kobayashi¹, A. Ono¹, N. Kimura¹ and O. Watanabe²

¹ Japan Atomic Energy Agency, Oarai, Ibaraki, Japan

² Mitsubishi FBR Systems Inc., Shibuya, Tokyo, Japan**

Abstract

Fully natural circulation system is adopted in a decay heat removal system (DHRS) of Japan Sodium Cooled Fast Reactor (JSFR). The DHRS of JSFR consists of one unit of DRACS (direct reactor auxiliary cooling system), which has a dipped heat exchanger in the reactor vessel and two units of PRACS, which has a heat exchanger in a primary-side inlet plenum of IHX in each loop. Sodium experiments were carried out for heat transfer characteristics of a sodium-sodium heat exchanger of PRACS and start-up transient of the DHRS loop with parameters of pressure loss coefficients in the loops. The transient experiments for the start-up of DHRS loop showed that quick increase of natural draft in the air duct followed by smooth increase of sodium flow rate in the DHRS loop. Influences of the pressure loss coefficients in the primary loop and the DHRS loop were limited on the core temperature and also heat removal of PRACS, respectively due to recovery of natural circulation head via the increase of temperature difference in each loop.

1. Introduction

The natural circulation is a significant issue on passive features of a sodium cooled fast reactor. Fully natural circulation system is adopted in a decay heat removal system (DHRS) of Japan Sodium Cooled Fast Reactor (JSFR) [1], which is developed by Japan Atomic Energy Agency in cooperation with Mitsubishi FBR Systems and Japanese electric power companies. The JSFR has two loops of the main heat transport systems. Then the DHRS of JSFR consists of two units of PRACS (primary reactor auxiliary cooling system), which has a heat exchanger in an inlet plenum of IHX and further one unit of DRACS (direct reactor auxiliary cooling system), which has a dipped heat exchanger in the reactor vessel. The decay heat after a reactor scram is removed solely by natural circulations in the primary loops and DHRS including natural draft in the air coolers. Such natural circulation DHRS is a key issue of the JSFR development project. Start-up and keeping the natural circulation are of importance for the decay heat removal.

A large scale sodium experiment, ILONA [2], was carried out for the DHRS of European Fast Reactor (EFR). EFR [3] has six dipped heat exchangers in the hot pool and air coolers of the DRACS. Sodium experiments were performed to verify component design of the air cooler and to investigate the steady state and transient behavior of natural convections of air and sodium. Heat removal capacity of the air cooer and transient behavior at the tube outlets during the start-up were confirmed to be within the permissible range. However, the experimental data is still

limited especially for the interactions among the primary loop, a DHRS sodium loop, and natural draft. Network analysis code was used to predict such natural circulations [4]. Pressure loss coefficients are significant input data for the analyses. However, the data have some errors or uncertainties especially under low flow velocity conditions in fuel subassemblies, sodium loop components, and also air flow paths. Influences of such pressure loss coefficients were mainly estimated by the analyses.

Sodium experiments were carried out to study the heat transfer characteristics, transient behavior of natural circulation in the DHRS of JSFR, and influences of pressure loss coefficients in sodium loops. A partial model of the straight tube type PRACS heat exchanger is installed in a sodium test loop named PLANDTL [5], which consists of a core simulator, a reactor upper plenum, the primary loop, and DHRS. Objectives of this study are to investigate the transient behavior of DHRS including the natural draft and to estimate the influences of pressure loss coefficients in the loops.

2. Decay heat removal system of JSFR

2.1 Design concept of DHRS

A flow diagram of the JSFR cooling system is shown in Fig. 1. The primary cooling system has only two loops in order to reduce number of components and reactor building space. An intermediate heat exchanger (IHX) and a primary pump are integrated into one component to reduce the component number and a cross-over leg of the primary cooling system. The steam generator (SG) is a straight tube type.

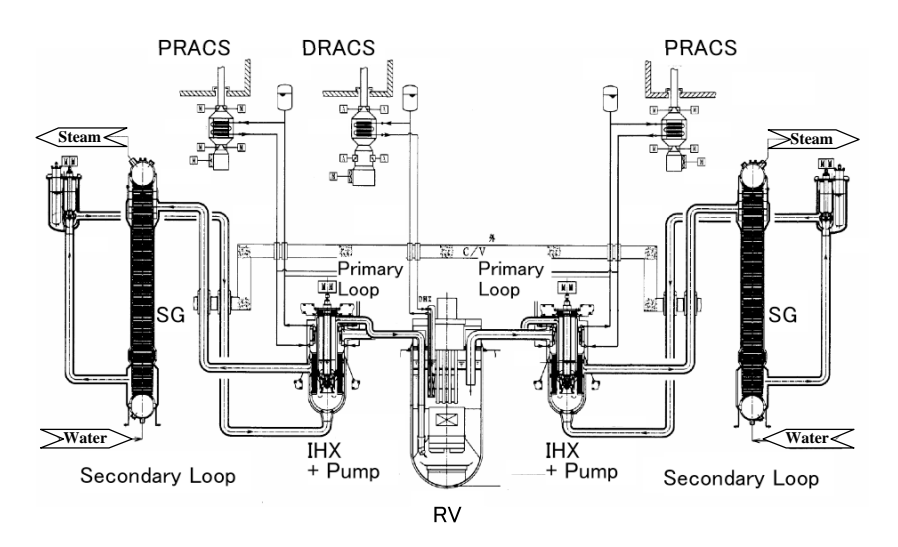


Fig. 1 Heat transport systems of JSFR

The DHRS of JSFR is a combined system using one unit of DRACS and two units of PRACS. A dipped heat exchanger is installed in the reactor upper plenum as DRACS. Further, a sodium-sodium heat exchanger is installed in the primary-side inlet plenum of each IHX as PRACS. There is no pony motor in the primary system. Further, no sodium pump nor air blower in the DHRS is connected to an emergency power supply. Thus, this DHRS is a fully

natural circulation system and natural circulation decay heat removal is demanded after a scram accompanied by loss of power incidents. In terms of diversity and redundancy, two independent dampers are installed at the inlet of each air cooler. Each of the dampers is driven by a motor, hence is an active component and connected to an independent emergency power line. Although the primary cooling system has only two loops, the coolant boundary is enclosed with a double-wall structure, so a risk to lose all of natural circulation paths of the primary loops is much reduced.

2.2 PRACS heat exchanger

The tubes of PRACS heat exchanger (PHX) are set outer side of the IHX inlet plenum, which is annular geometry. There is large flow area beside the PHX tubes for the primary loop flow. However, this tube arrangement may cause a bypass flow during the operation of PRACS. Local natural convection in the IHX inlet plenum is developed by the cooling of PHX. Further, the main flow in the primary loop is decided by not only the cooling of PHX, but the temperature distribution along the entire primary circuit. Thus, this primary loop flow can overcome the local flow through the PHX tube bundle and make the bypass flow. In this case, the heat transfer characteristics of the PHX will depend on the ratio of bypass flow to the primary flow. Further, temperature distribution across the IHX inlet plenum is also of importance on the structural integrity.

2.3 Operation of DHRS

During standby operation under full power condition of the reactor, the sodium flow in the DHRS loop is maintained by natural circulation and heat loss in the air cooler. The dampers limit natural draft in the air cooler so as to minimize the heat loss and also keep certain sodium flow rate.

When the reactor is shut down and the DHRS is demanded, the dampers of air cooler are opened and natural draft starts. Natural circulation flow rate in the DHRS sodium loop is increased by the temperature decrease in the air cooler and finally the primary loop flow is kept by the heat removal of the DHRS.

3. Sodium loop and test section

3.1 Test loop

A sodium test loop, PLANDTL, is used to investigate the transient phenomena in the DHRS and also the heat transfer characteristics of PHX. Figure 2 shows schematic of the test loop. It consists of a simulated core, a reactor upper plenum, the primary loop, IHX, a lower plenum, the secondary loop, a main air cooler instead of a steam generator, a DHRS loop, and an air cooler of DHRS. A dipped heat exchanger (DHX) is installed in the reactor upper plenum. The PLANDTL loop was originally designed to simulate thermal hydraulics in the core during transition from forced to natural circulation. A partial and axially full-scale model of core fuel subassemblies was installed. The primary loop was designed to give appropriate boundary

conditions to the simulated core. So, the height in the primary loop was scaled down with respect to a design of sodium-cooled reactor in 1990'.

A partial model of PHX was newly installed in the primary side inlet plenum of IHX to simulate DHRS of JSFR. The DHRS loop in the PLANDTL can select the DHX or PHX as the sodium heat exchanger by valves in the loop. The height difference between the PHX and the air cooler in the DHRS loop is 1/7 of that in JSFR. The air stack height from the DHRS air cooler is nearly 1/8 of that in JSFR. The pipe diameter of the DHRS loop is also 1/8 of that of JSFR. The core model has 7 subassemblies and a 37-pin bundle in the center subassembly, where the surface heat flux on each the fuel pin is simulated by an electric heater. The pin diameter and pitch are modeled with nearly 1/1 scale of a reactor. The heated length is 1m and the same as in a reactor. The center subassembly is a full scale partial model. Total power of the core is 1MW at the maximum. The pin surface heat flux in the central subassembly reaches around 12% of full power condition in a core fuel subassembly.

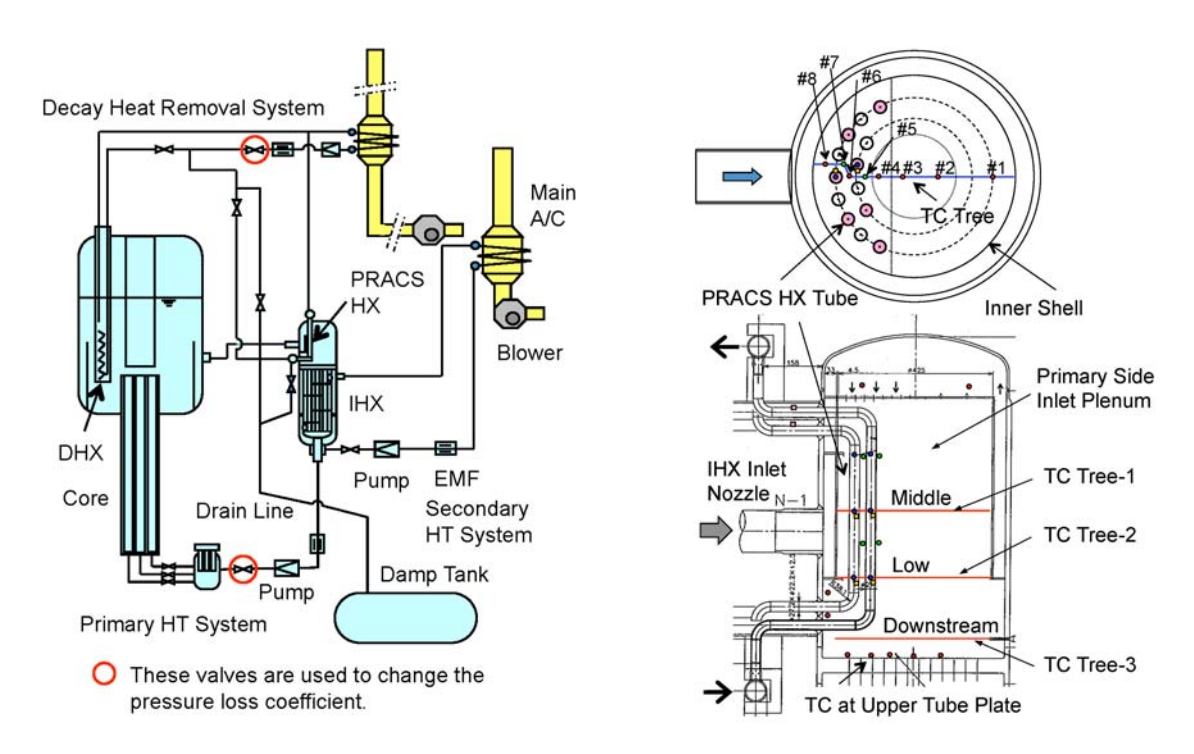


Fig. 2 Flow diagram of PLANDTL

Fig. 3 PRACS heat exchanger (PHX) in IHX

The IHX is a shell and tube type heat exchanger and the primary coolant flows through the inside of the tubes. The tube length is around 1/6 of that in JSFR. Further, the height difference between the center of the heated core length and center of the PHX is around 1/6 of those in JSFR. The height scales of the core, IHX, and the primary loop are different. Thus, this test loop can not simulate accurate transient of the natural circulation in the primary loop of JSFR. However, the scales of height differences among the core, the PHX, the DHRS air cooler, and the air stack are nearly the same value of 1/6 to 1/8. Thus, basic phenomena during the start-up of natural circulations from the air stack, the DHRS loop and the primary loop can be investigated in this test facility.

3.2 PRACS heat exchanger (PHX) model

Figure 3 shows schematic of the PHX model in the IHX. In order to evaluate heat transfer characteristics of PHX, the Pe number similarity is required. A scaled model results in too small Pe as compared with that in JSFR. The PHX tube arrangement is modeled partially. Two layers of the tubes are set near the inner shell wall. There is a wide flow area beside the tubes. The tube outer diameter is 27.2mm and only 15% smaller than that in JSFR. The ratios of tube pitch by diameter in circumferential and radial directions are nearly the same as those in JSFR. Local natural circulation in the IHX inlet plenum will develop along the PHX tubes. Thus longer tube length is desired. However, vertical tube length is 0.59m and around 1/3 of that in JSFR due to space limitation. Influences of the tube length are discussed in Section 4.2.

As for the natural circulation through the DHRS loop, the head is governed by the height difference between the PHX and the air cooler. When the Ri number similarity is assumed in the DHRS loop with this length scale of 1/8, the power ratio is estimated under the same temperature condition as in JSFR as follows,

$$Ri = \frac{g \beta \Delta T L}{u^2}$$

$$(Ri) = \frac{(L)}{(u)^2} = 1$$
(1),

$$Q = \rho C_p \Delta T u L^2$$

$$(Q) = (u)(L)^2 = (L)^{2.5}$$
(2).

Here, a bracket means a ratio of model to reactor. When (L) is 1/8, (Q) becomes 1/180. The heat removal capacity of the PHX should be 130kW in the model. The heat transfer area, i.e., tube number was set so as to obtain this heat removal capacity.

3.3 Measurement system

Temperatures in the IHX inlet plenum are measured by thermocouples of 0.5mm diameter (Chromel-Alumel, sheathed ungrounded type). The measurement positions are shown in Fig. 3. Transverse distributions across the PHX tubes and the flow area beside the tubes are measured at several heights. The measurement errors of the thermocouples were less than 0.2°C based on relative calibration in a temperature range between 300 and 500°C. Flow rates in the loops are measured by electromagnetic flow meters. The calibrations were done based on tank volume between two level meters and time differences during a sodium drain from the tank. The estimated standard deviations of error were 0.76 and 0.07 l/min in the primary loop and the DHRS loop, respectively. Typical flow rates of natural circulations were 40 and 25 l/min in the primary loop and the DHRS loop, respectively.

4. Thermal hydraulic characteristics of PHX

4.1 Experimental parameters

Steady state experiments were carried out to obtain the heat transfer characteristics of the PHX and temperature distributions across the IHX inlet plenum. The primary flow rate was a main experimental parameter to investigate the influence of the bypass flow. The natural circulation flow in the JSFR primary loop was predicted by a network analysis and also a water experiment [6]. The estimated flow rate is 3% of full power flow rate. The average flow velocity in the IHX inlet annulus is 0.04 m/s in JSFR according to this flow rate. The parameter range of the primary flow rate in the experiment was decided to cover the average velocity of 0.04 m/s as shown in Table 1.

The sodium flow rate in the PRACS loop was kept at constant by the electromagnetic pump. The primary side inlet temperature to PHX was maintained at 490°C. The primary loop flow rate was varied from 50 to 600 l/min. The case name of PFxxx or Pxxx means that the primary side flow rate is xxx l/min. The air flow rate was controlled so as to maintain the sodium outlet temperature of the air cooler by using the blower.

Case	Flow rate (l/min)		Flow velocity in	Temperature* (°C)	
	Primary PRACS		inlet plenum (m/s)	Primary	PRACS
PF100	97	82	0.012	493	376
PF200	201	81	0.025	491	376
PF300	300	80	0.037	489	376
PF400	392	82	0.049	486	376
PF500	493	81	0.061	490	376
PF600	590	81	0.073	490	376
P100D80	97	78	0.012	482	376
P100D60	99	59	0.012	480	356
P100D40	97	40	0.012	486	354
P200D80	196	78	0.024	486	376
P150D80	149	78	0.019	487	376
P50D80	44	76	0.006	484	376
P50D60	47	58	0.006	485	356

Table 1 Experimental conditions of steady state experiments

4.2 Temperature distribution and heat transfer characteristics of PHX

The heat transfer characteristics on the shell side are of importance for the design of PHX. Thus, the flow velocity around the PHX tubes should be known. Figure 4 shows the transverse temperature distributions at three heights across the IHX inlet plenum (see Fig. 3) in three cases of PF100, PF300, and PF600. The sodium temperature at the middle height of PHX tubes showed dip around the PHX tubes. It means that some amount of the primary loop flow

^{*} Inlet temperature into PHX

bypassed the PHX tubes. At the lower position in the tubes, the higher flow rate resulted in the larger temperature dip near the PHX tubes. In the low flow rate case of PF100, the temperature in the entire area had nearly flat distribution and was lower than in other cases. This means that the temperature distribution was flattened by convection due to buoyancy force, which was relatively larger than inertia force of the decreased primary flow. The local temperature reductions in the higher flow rate cases remained at the downstream position from the PHX tubes and reached the upper tube plate of IHX.

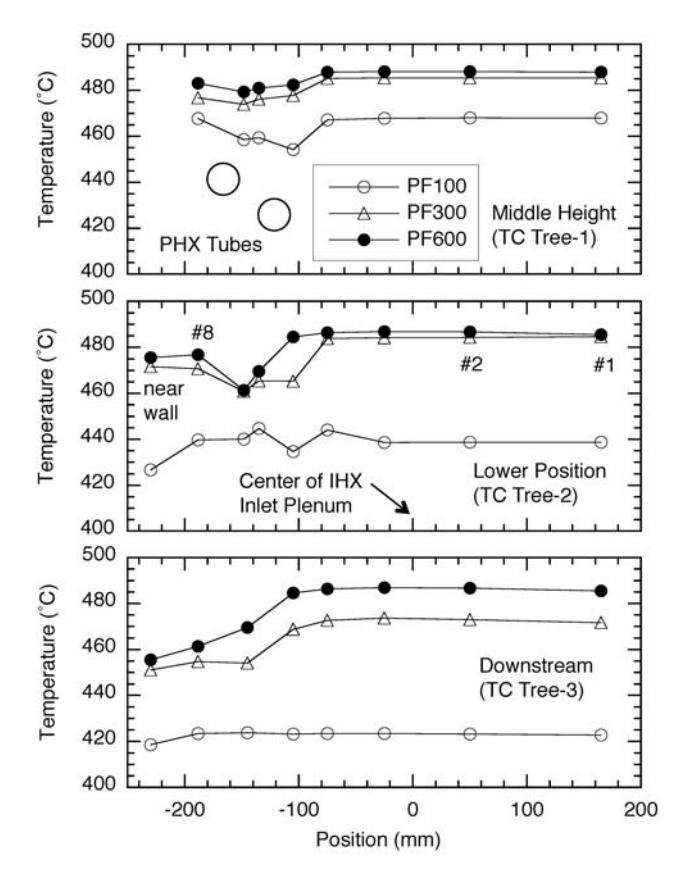


Fig. 4 Transverse temperature distributions across PHX tubes and IHX inlet plenum

In order to account such bypass flow, the flow rate through the PHX tube bundle was estimated according to heat balance between the primary flow and the DHRS loop flow. The temperature at PHX downstream position was used as the primary side PHX outlet temperature. The flow area through the PHX tube bundle was supposed as follows. The outer boundary was set at the inner shell wall of the IHX. The inner boundary was set at circular arc apart from the PHX tubes by a half pitch of tube bundle arrangement, and the side boundaries at radial line apart from the outermost tubes by the half pitch. The flow velocity through the tube bundle, V_o , was obtained from the estimated flow rate based on the heat balance and the flow area. The equivalent hydraulic diameter was obtained from this flow area and perimeter length, D_o =0.0405m. The shell side Pe number is defined as follows,

$$Pe = \frac{V_o D_o}{\alpha} \tag{3}.$$

The heat transfer coefficient on the shell side was obtained from the overall heat transfer coefficient and the heat transfer coefficient on the tube inside wall. The heat transfer coefficient on the tube inside wall was evaluated based on the correlation of Seban-Shimazaki as follows.

$$Nu = 5.0 + 0.025 Pe^{0.8}$$

$$h_i = Nu \frac{\lambda}{D_i}$$
(4).

The overall heat transfer coefficient was estimated by inlet and outlet temperatures of the primary side flow and the DHRS loop flow into PHX. The outlet temperature of the primary side flow was defined at the IHX primary side outlet. The IHX secondary loop was closed by a valve and the IHX outlet temperature and average of IHX upper tube plate temperatures below the PHX tubes were in good agreement. Thus, the IHX primary side outlet temperature was used as the outlet temperature of PHX.

The obtained heat transfer data in cases of PF100 and 300 are shown in Table 2. In case of the lower primary flow rate of PF100, the estimated flow rate through the PHX tube bundle was nearly equal to the primary flow rate. However, it was 78% in the higher primary flow rate case of PF300.

Item	PF100	PF300
Average velocity in IHX inlet plenum (m/s)	0.012	0.037
Heat removal of PRACS (kW)	126	141
PHX bundle flow rate ratio based on heat balance	1.0	0.78
Estimated velocity around PHX tube bundle (m/s)	0.08	0.21
Pe number in primary side	62	153
Heat transfer coefficient on tube outside (W/m ² K)	7600	7900

Table 2 Heat transfer data

The shell side heat transfer coefficients are shown in Fig. 5 with a heat transfer correlation of Lubarsky-Kaufman, which has been used in the JSFR design study as shown below.

$$Nu = 0.625 Pe^{0.4}$$

$$h_o = Nu \frac{\lambda}{D_o}$$
(5).

The experimental data were well correlated with the design correlation in higher Pe number conditions. The estimated Pe in JSFR under natural circulation condition is 100 to 300 (D_0 =0.053m). Even in lower Pe condition, the data points were on a curve and slightly larger than the design correlation (+15% at Pe=100). This means that the design correlation has some margin in low Pe region and is adequate for the evaluation of the heat transfer characteristics of PHX.

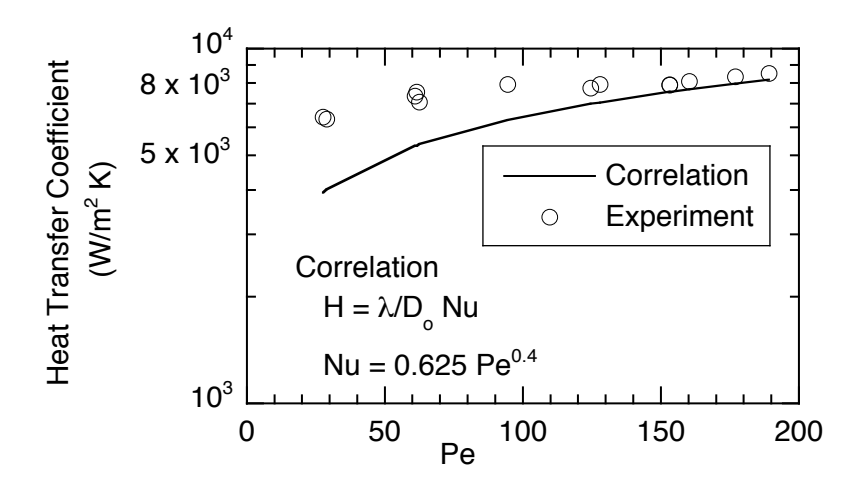


Fig. 5 Shell side heat transfer coefficient of PHX

5. Transient behaviour of natural circulation DHRS

5.1 Concept of transient experiment

Transient characteristic in the primary system depends on those in the secondary system and also the decay heat removal system (DHRS). Heat transfer in the heat exchangers between these systems is significant for such interactions. Thus the sodium experiments are required to simulate the higher heat transfer, which can not be simulated in a water system, and also the transient behaviour including the interaction between the heat transport systems.

In the experiments, start-up of the natural circulations in the primary loop and the DHRS including the natural draft in the air stack were investigated with parameters of pressure loss coefficients in the sodium loops. The natural circulation flow course depends on the loop geometry and is not simulated precisely due to the limitations of geometry similarity. However, mechanism of the interactions is well examined by the sodium experiments.

5.2 Experimental conditions

The experiments were carried out to investigate the transient behaviour of natural circulation in the DHRS with the parameter of pressure loss coefficients in the sodium loops. The initial condition in the primary loop is 6% flow velocity in the center subassembly and 6% core power as compared with the full power condition of a core fuel pin heat flux. The Re number in the pin bundle is nearly 3,000 under forced convection. Transient curves of flows and power are shown in Fig. 6. The heater power of the core was reduced quickly from 6% (500kW) to 1.8% (150kW) at t= 0 to 1s and kept at 1.8%, which simulated the decay heat level around 1000s from the reactor scram. The primary pump stopped at t=90s from the scram and then the natural circulation started. The secondary loop flow was also reduced and switched to natural circulation. The dampers of main air cooler in the secondary loop were closed at t=90s after the stop of air blower. However, the air leak flow continued through the dampers. The valve in

the secondary loop was closed at 2030s in order to stop the natural circulation because of no heat sink in the secondary loop after the scram in JSFR.

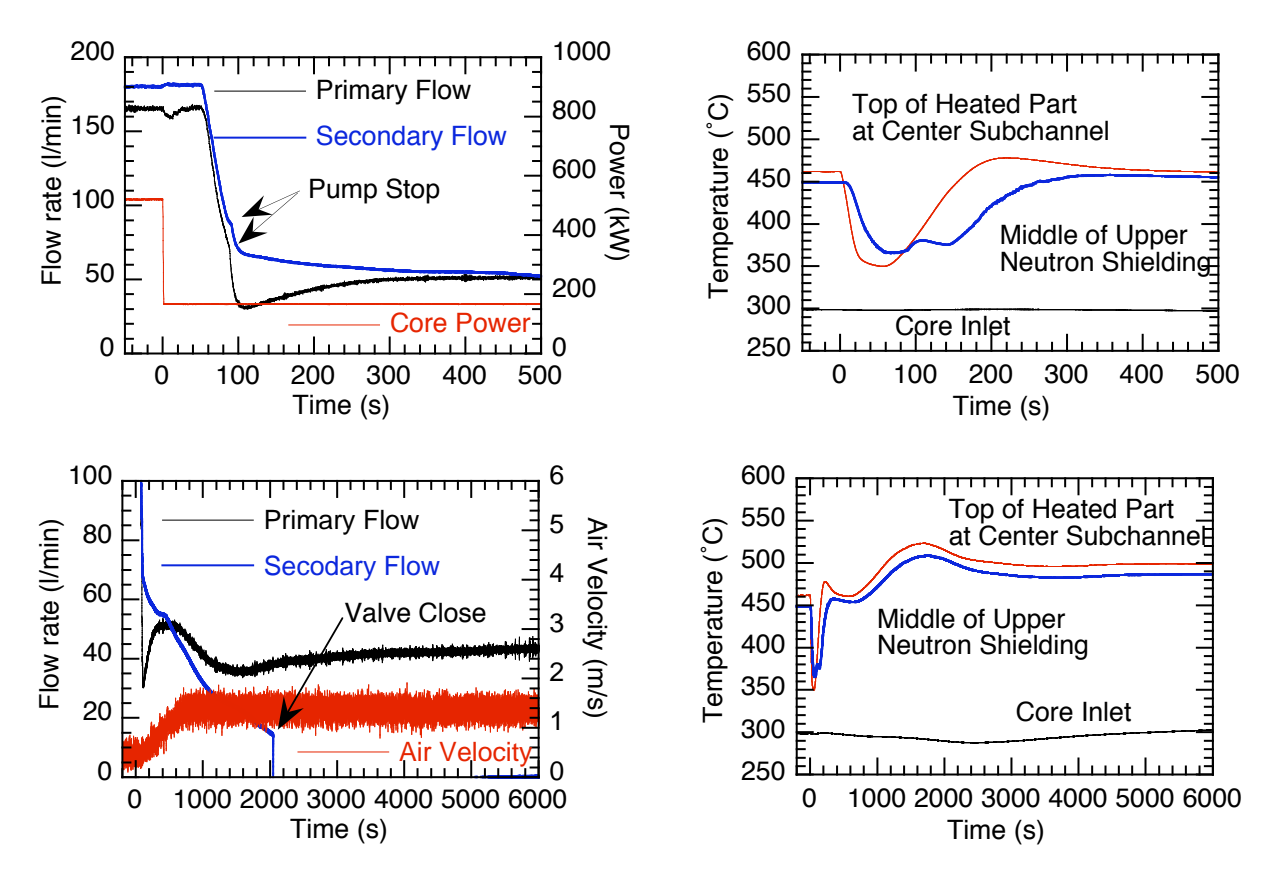


Fig. 6 Time trends of primary and secondary flow rates and core power

Fig. 7 Time trends of core temperatures

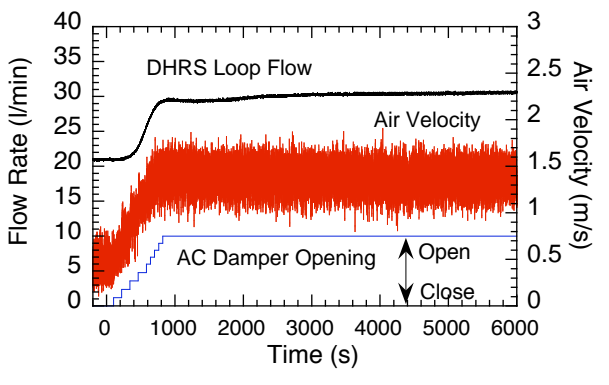
The inlet damper of the DHRS air cooler was opened gradually during t=100 to 800s in order to mitigate thermal shock in the DHRS loop. The outlet damper was opened at t=100s. A blower of the air cooler and a sodium pump of the DHRS were not operated during the entire transient. The opening of the air dampers began the natural draft through the air cooler and the air stack.

The pressure loss coefficients were varied by the valve opening in the primary loop and the sodium loop of DHRS (see Fig. 2). The pressure loss characteristics in the primary loop and DHRS loop were obtained from the pressure loss and flow rates in the preliminary experiments under forced flow and homogeneous temperature conditions.

5.3 Transient phenomena in basic case

The sodium temperature at the heated end of center subchannel in the central subassembly is shown in Fig. 7 as the highest temperature in the simulated core together with the subassembly inlet temperature in short and long terms. The highest temperature in the core showed the so-called second peak at t=220s after some delay from the pump stop due to fluid transportation

along the heated length and heat capacity. After that, the temperature was decreased due to the development of natural circulation flow rate as shown in Fig. 6. At t=1500s the third peak was registered. The flow rates in the primary and secondary loops were shown in Fig. 6 of long-term. The temporal decrease of the primary loop flow rate due to reduction of natural circulation head via loss of heat sink in IHX resulted in the third peak of the core temperature.



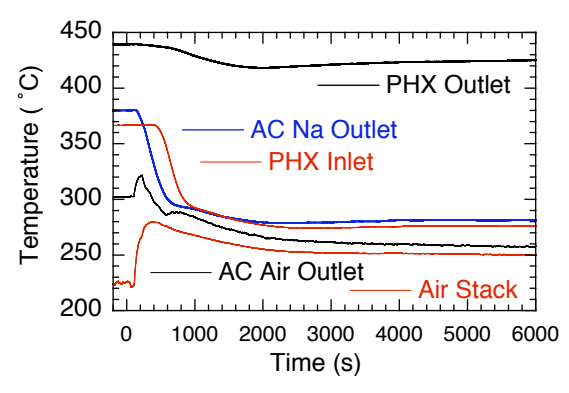


Fig. 8 Air velocity and DHRS loop flow rate

Fig. 9 DHRS loop and air temperatures

Air velocity in the air cooler duct and DHRS loop flow rate are shown in Fig. 8 together with the The air velocity increased immediately corresponding to the air damper inlet damper opening. opening. However, the sodium flow rate in the DHRS loop increased 100s behind from the change of the air velocity. The sodium velocity in the DHRS loop was slower than the air This caused longer transportation delay of the cold fluid in downward flow path of the DHRS loop and slower increase of the natural circulation head. Figure 9 shows the air temperatures at just outlet of the air cooler and at the middle height of air stack and the sodium temperatures of the air cooler and the PHX. The delay of the sodium temperature drop at the PHX inlet (the end of downward flow path in the DHRS loop) was confirmed as compared with the air temperature responses. Opening procedure of the air cooler dampers should be decided so as to mitigate the thermal shock due to excess temperature decrease via the time delay of DHRS sodium flow. The PHX inlet temperature was slightly lower than the air cooler outlet sodium temperature. This temperature reduction was resulted from heat loss in the DHRS loop.

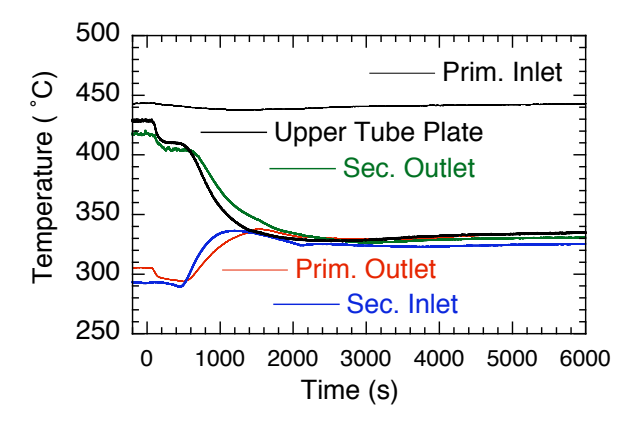


Fig. 10 Trends of IHX inlet and outlet temperatures

The temperatures around IHX are shown in Fig. 10. The primary side outlet temperature decreased by 15°C just after the scram due to the loss of the flow rate and heat exchange with the low temperature fluid in the shell side. At t=500s, the primary side outlet temperature increased due to the loss of heat removal in the secondary loop. However this temperature increase stopped at t=1600s due to the heat removal of PHX. The upper tube plate temperature of IHX was also decreased by the heat removal of PHX and the entire length of IHX tube was kept at low temperature level. This temperature reduction at higher position of downward flow path caused the recovery of the primary loop flow rate at 1500s as shown in Fig. 6.

6. Influences of pressure loss coefficients in the loops

6.1 Pressure loss variation in the primary loop

The pressure loss coefficient, Kp, in the primary loop was varied by the valve opening at three levels as shown in Table 3. Figure 11 shows the time trends of the primary loop flow rates in the reference case of 100% valve opening (Case Ref-p) and also the case of 25% opening (Case Kp+40) where the pressure loss coefficient increased by 40% as compared with that in Case Ref-p. The flow rate in Case Kp+40 was lower than in Case Ref-p, however, the reduction was only 7 to 10%. If the driving force of the natural circulation head was the same with that in the reference case, the flow rate should be reduced by 18% according to the following pressure balance.

$$\Delta P = K \frac{1}{2} \rho u^2 \tag{6}.$$

Table 3 Experimental conditions and results of primary loop parameter cases

Case	Valve	Pressure	Primary	Temperature	Temperature
	Opening	Loss	Flow Rate	Increase at	Increase at 3rd
	(%)	Coefficient	at 1500s	2nd peak (°C)	peak (°C)
Ref-p	100	Reference	Reference	179	232
Kp+20	36	+20%	- 4%	188 (+5%)	240 (3%)
Kp+40	25	+40%	- 7%	196 (+10%)	246 (6%)

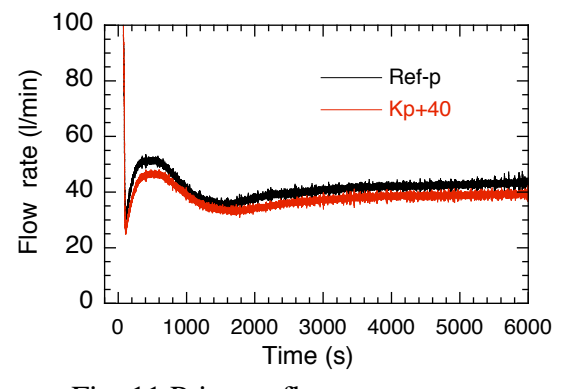


Fig. 11 Primary flow rate courses

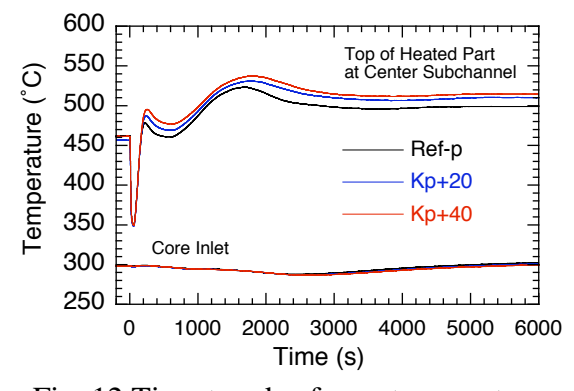


Fig. 12 Time trends of core temperature

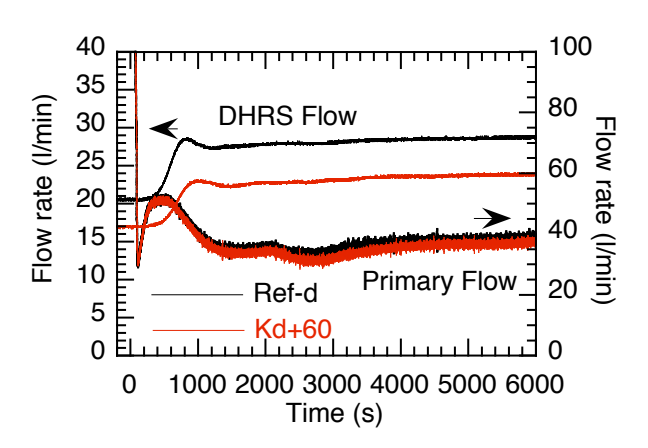
Core temperatures are shown in Fig. 12. The temperature increase at the top of heated length from the core inlet in Case Kp+40 was larger by 10% at the second peak and 6% at the third peak than in Case Ref-p. This higher temperature in the core increased the natural circulation head and resulted in relatively smaller decrease of the flow rate. This recovered flow rate also contributed to mitigate the core peak temperatures. As a result, the core temperature increase was only 10% in spite of the 40% increase of the pressure loss coefficient due to the feed back of flow rate and core temperatures.

The core temperatures in Case Ref-p, Case Kp+20, and Case Kp+40 are shown in Table 3. In Case Kp+20, the core temperature increases at the second and third peaks were larger by 5% and 3% respectively than in Case Ref-p. Thus, the temperature increases were nearly half of these in Case Kp+40.

These correlations among the pressure loss coefficients, flow rates, and the core temperatures can not be applied to reactors directly. However, they gave significant insights of the pressure loss coefficients and code validation database.

6.2 Pressure loss variation in the DHRS loop

The pressure loss coefficient in the DHRS loop was varied to see its influence on the heat removal performance. The valve opening in the DHRS loop was set at 100% and 25%. The pressure loss coefficient in the case of 25% valve opening (Case Kd+60) increased by 60% as compared with the reference case (Case Ref-d) of 100% opening. The damper opening in the air flow path was limited at a fixed value to keep the air cooler outlet sodium temperature above 250°C in both cases.



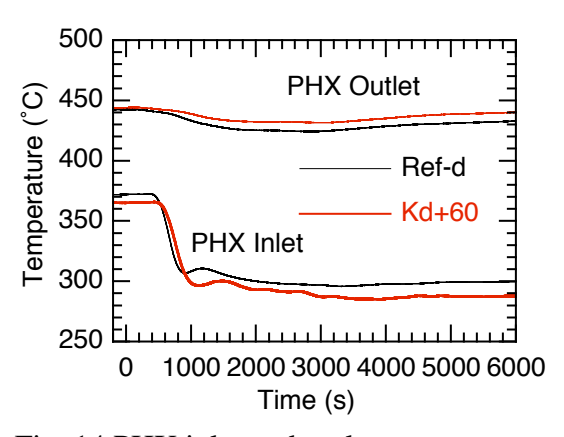


Fig. 13 Primary and DHRS loop flow rates

Fig. 14 PHX inlet and outlet temperatures

Figure 13 shows the flow rates in the primary loop and the DHRS loop. The flow rate in the DHRS loop in Case Kd+60 was smaller by 18% than in Case Ref-d at the initial standby operation due to 60% increase of the pressure loss coefficient. After the damper opened, the DHRS loop flow rate increased, however, the flow rate in Case Kd+60 was still smaller by 17% than in Case Ref-d. Flow development in Case Kd+60 was also slower than in Case Ref-d due to the larger transportation delay through the DHRS loop. The primary loop flow rate in the Case Kd+60 was slightly smaller than in Case Ref-d after 1000s.

The inlet and outlet temperatures of PHX are shown in Fig. 14. The PHX inlet temperature in Case Kd+60 was lower by 5°C than in Case Red-d at the initial standby operation due to the lower flow rate in the DHRS loop as shown in Fig. 13. After the scram, the PHX outlet temperature in Case Kd+60 decreased, and was still lower than in Case Red-d. On the other hand, the PHX outlet temperature after the scram in Case Kd+60 was slightly higher than in Case Ref-d. Lower flow rate in the DHRS loop resulted in larger temperature increase in the PHX secondary side.

Figure 15 shows the inlet and outlet temperatures of the IHX primary side and also the sodium temperature at the IHX upper tube plate. The temperatures at the tube plate decreased due to the cooling by PHX. However, the temperature in Case Kd+60 was higher by nearly 10°C than in Case Ref-d due to reduction of heat removal of PHX. The IHX outlet temperature was also higher in Case Kd+60 after 2200s than in Case Ref-d due to loss of heat sink in the IHX secondary loop and the reduction of heat removal of PHX.

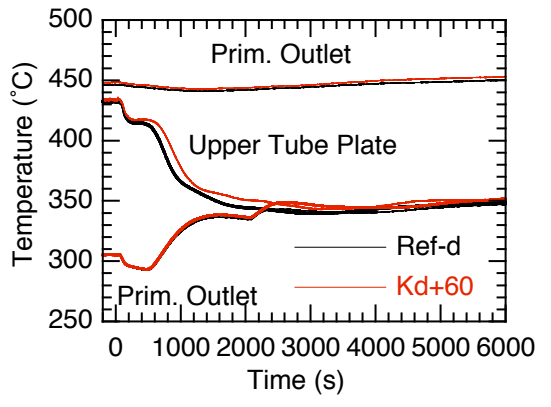


Fig. 15 IHX primary side inlet and outlet temperatures

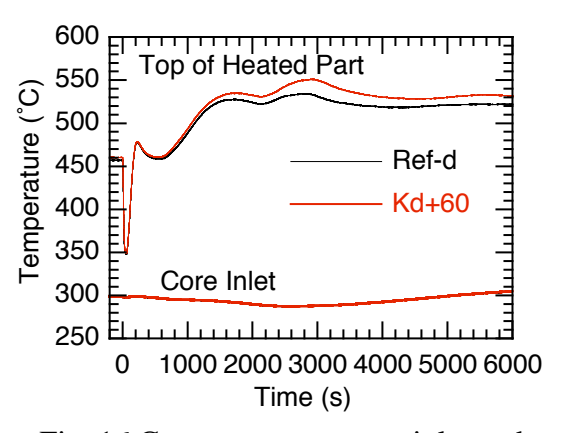


Fig. 16 Core temperatures at inlet and top of heated part

These flow rates and IHX temperatures influenced the core temperatures. Figure 16 showed the temperatures at the center subassembly inlet and the highest temperature position of the top of heated length in the center subchannel. The core inlet temperatures were nearly identical between two cases. However, the temperature at the top of heated length in Case Kd+60 was higher by 10 to 20°C than in Case Ref-d after 1000s. The reason is reduction of the primary loop flow rate as shown in Fig. 13. The primary loop flow rate was decreased by the reduction of natural circulation head, i.e., higher temperature increase at the IHX primary side as shown in Fig. 15. However, the influence on the core temperature was less than 10% of temperature increase in the core in spite of the 60% increase of pressure loss coefficient in the DHRS loop.

The flow rates, PHX heat removal are summarized in Table 4. The heat removal in PHX in Case Kd+60 was reduced by 9% as compared with that in Case Ref-d at initial state of standby operation and by only 5% at the fully developed state (6000s). The heat removal was compensated by the temperature decrease at the air cooler outlet because of the nearly same heat removal at the air side which was decided the temperature difference between air and sodium flows and air side flow resistance.

Table 4 Experimental	conditions a	and results of	f DHRS 10	oop cases
1 00010 . =p 0111110111001	. • • • • • • • • • • • • • • • • • • •	************		30 p •••5•5

Case	Valve	Pressure loss coefficient	DHRS loop flow rate (I/min)		PHX removal heat (kW)	
	opening (%)		Standby operation	t=6000s	Standby operation	t=6000s
Ref-d	100	Reference	21	29	21	69
Kd+60	25	+60%	17 (-18%)	24 (-17%)	19 (-9%)	66 (-5%)

7. Conclusions

Sodium experiments on the heat transfer characteristics and natural circulations in DHRS were performed. The straight tube type heat exchanger of PRACS was installed in the sodium test facility, PLANDTL. The heat exchanger tubes are set at one-side and large flow area is formed beside the tubes in the IHX inlet plenum. Several transient experiments were carried out from forced circulation in the primary loop and standby operation of DHRS to the natural circulations. Pressure loss coefficients in the primary loop and DHRS loop were varied to examine influences on heat removal capability. Following conclusions were obtained.

- 1) Temperature distribution across the IHX inlet plenum had local dip around PHX tubes under high flow velocity condition in the plenum due to the bypass flow. Heat transfer characteristics of PRACS heat exchanger (PHX) tubes were obtained. The heat transfer coefficient on the shell side can be estimated by a conventional correlation.
- 2) The start-up of natural circulations was smooth in the air duct of the air cooler, DHRS loop, and the primary loop. Time delay of start-up of natural circulation was found in the DHRS loop as compared with that in the air duct.
- 3) The pressure loss coefficients in the primary loop and DHRS loop influenced the natural circulation flow rates in the loops directly. However the decreases of the flow rates were limited and compensated with increase of temperature differences in the loops, namely natural circulation head. The 60% increase of pressure loss coefficient in the DHRS loop resulted in only 5% reduction of the heat removal in PHX.

This paper describes the outlines of results obtained from the sodium tests, which were conducted in a study of "Development of evaluation methods for decay heat removal by natural circulation under transient conditions" entrusted to "MITSUBISHI FBR SYSTEMS, INC. (MFBR)" by the Ministry of Education, Culture, Sports, Science and Technology of Japan (MEXT). The sodium experiments were performed by Japan Atomic Energy Agency (JAEA) under the contract with MFBR.

Acknowledgements

The authors are grateful to Mr. T. Koga and Dr. Y. Eguchi of CRIEPI and Mr. M. Sato of MFBR for useful discussions of natural circulation phenomena and component design of FBR. The authors also wish to express their gratitude to Mr. M. Sumiya and operation staffs of the sodium test loop.

Nomenclature

C_p	specific heat of fluid	[J/kg K]
$\mathbf{D_i}$	inner diameter of PHX tube	[m]
D_{o}	hydraulic equivalent diameter in shell side of PHX	[m]
g	gravitational acceleration	$[m/s^2]$
h	heat transfer coefficient	$[W/m^2 K]$
K	pressure loss coefficient	[-]
L	representative length	[m]
Q	power of simulated core	[W]
u	representative velocity	[m/s]
V_{o}	velocity through tube bundle	[m/s]

Greek Letters

α	thermal diffusivity	$[m^2/s]$
β	coefficient of thermal expansion	[1/K]
ΔT	temperature difference	[K]
ΔP	pressure loss	[Pa]
λ	thermal conductivity of fluid	[W/m K]
ρ	density of fluid	$[kg/m^3]$

References

- [1] Kotake, S., Sakamoto, Y., Mihara, T., et al., "Development of advanced loop-type fast reactor in Japan," Nuclear Technology, Vol.170, 2010, pp.133-147.
- [2] Stehle, H., Damm, G., and Jansing, W., "Large scale experiments with a 5MW sodium/air heat exchanger for decay heat removal," Nuclear Engineering and Design, Vol.146, 1994, pp.383-390.
- [3] Hennies, H.H., Leduc, J., and Goddard, S.C., "Development of Fast Reactors in Europe," <u>Proc. Int. Conf. on Fast Reactors and Related Fuel Cycles (FR91)</u>, Vol.1, pp.1.2-1to11, Kyoto, Japan, 1991, Oct. 28-Nov. 1.
- [4] Yamaguchi, A., et al., "Plant wide thermal hydraulic analysis of natural circulation test at Joyo with MK-II irradiation core," <u>Proc. of 4th Int. Top. Mtg. on Nuclear Reactor Thermal-Hydraulics (NURETH-4)</u>, Vol.1 p.398, Karlsruhe, F.R. Germany, 1989.
- [5] Kamide, H., Kobayashi, J., Ono, A., et al., "Sodium experiments on decay heat removal system of Japan sodium cooled fast reactor," NTP0057, Chuncheon, Korea, 2010, Nov.14-17.
- [6] Ohyama, K., Watanabe, O., Eguchi, Y., Koga, T., et al., "Decay Heat Removal System by Natural Circulation for JSFR," <u>Proc. of Int. Conf. on Fast Reactors and Related Fuel Cycles (FR09)</u>, 08-21P, Kyoto, Japan, 2009, Dec. 7-11.